Chemistry of Metals and Alloys

Chem. Met. Alloys 3 (2010) 208-219
Ivan Franko National University of Lviv
www.chemetal-journal.org

Phase equlibria in the {Y, Gd}–Ni–Al ternary systems in the 65-100 at.% Al range at 773 K: a reinvestigation

Taras MIKA[1], Bogdan KOTUR[1]*

[1] *Department of Inorganic Chemistry, Ivan Franko National University of Lviv, Kyryla i Mefodiya St. 6, UA-79005 Lviv, Ukraine*
* *Corresponding author. E-mail: kotur@franko.lviv.ua*

Received September 13, 2010; accepted October 29, 2010; available on-line February 15, 2011

The phase equilibria in the Al-rich region of the {Y, Gd}–Ni–Al ternary systems at 773 K have been reinvestigated using XRD, microstructure and X-ray microprobe analysis. Four intermetallic compounds: 1 - $R_3Ni_5Al_{19}$ (structure type $Gd_3Ni_5Al_{19}$), 2 - $R_4Ni_6Al_{23}$ ($Y_4Ni_6Al_{23}$), 3 - RNi_3Al_9 (YNi_3Al_9) and 4 - $RNiAl_4$ ($YNiAl_4$), exist in both systems. It was shown that the thermodynamic equilibrium state of the samples could be reached after a relatively long heat treatment (up to four months). This is probably the main reason for some contradictions in the literature on the {Y, Gd}–Ni–Al phase diagrams. The crystal structure of the $Y_3Ni_5Al_{19}$ ternary compound ($Gd_3Ni_5Al_{19}$ type, space group *Cmcm*) was refined by the Rietveld method from powder X-ray diffraction data. The refined cell parameters are a = 0.40713(1) nm, b = 1.5957(3) nm, c = 2.7052(6) nm.

Rare-earth ternary systems / Phase equilibria / Intermetallic compounds

Introduction

In addition to a number of practical applications, rare-earth elements (*R*) are also used as modifying agents for different metallic alloys. Amorphous metallic alloys (AMA) based on Al and doped with rare-earth and/or transition (*M*) elements exhibit better corrosion resistance and mechanical properties than their crystalline analogues [1]. Thermal treatment of AMA causes their crystallization, which takes place in a few steps. By carrying out partial crystallization of AMA, one can change their properties, *e.g.* mechanical, chemical and others. We have recently studied the influence of Gd and Fe on the crystallization of $Y_5Ni_8Al_{87}$ AMA [2]. The crystallization of $Y_5Ni_8Al_{87}$, $Y_4Gd_1Ni_8Al_{87}$ and $Gd_5Ni_8Al_{87}$ leads to precipitation of Al(*R*) and $R_3Ni_5Al_{19}$ (structure type $Gd_3Ni_5Al_{19}$) (*R* = Y, Gd). Al(*R*) and RFe_4Al_8 (structure type $CeMn_4Al_8$) crystallize in AMA with Fe ($Y_4Gd_1Ni_4Fe_4Al_{87}$ and $Gd_5Ni_4Fe_4Al_{87}$). In order to better understand the crystallization processes in amorphous alloys, a comparison of the results of AMA devitrification with the phase equilibrium state of the corresponding solids is required.

Literature data on the phase diagrams of the binary *R*–Al, Ni–Al and ternary (Y, Gd)–Ni–Al systems is summarized below.

Binary systems. The investigated parts of the ternary systems are limited by the binary systems Ni–Al, Gd–Al and Y–Al. Two binary intermetallic compounds (IMC) are formed in the Al-rich region in each of these systems. Their crystal structure characteristics are presented in Table 1.

Ternary systems. The phase equilibria in the {Y, Gd}–Ni–Al ternary systems at 1073 K have been investigated in the whole concentration range [8,9]. Two ternary compounds RNi_3Al_{16} (orthorhombic) and $RNiAl_4$ (structure type $YNiAl_4$) (*R* = Y, Gd) have been reported within the 60-100 at.% Al range. Further investigations [10-14] did not confirm the RNi_3Al_{16} IMC, but three new ternary compounds, YNi_3Al_9, $Y_4Ni_6Al_{23}$ and $Gd_3Ni_5Al_{19}$ with own structure types, were found. The structure types $Y_4Ni_6Al_{23}$ and $Gd_3Ni_5Al_{19}$ are related and belong to the structure series $R_{4+m}M_{2+m}Al_{15+4m}$ [11]. Crystallographic data for the Al-rich IMC in the {Y, Gd}–Ni–Al ternary systems are presented in Table 2.

Vasiliev *et al.* [16,18] observed the coexistence of $R_4Ni_6Al_{23}$ and $R_3Ni_5Al_{19}$ in some ternary alloys of the {Y, Gd}–Ni–Al systems. They consider these compounds as polymorphic modifications, taking into account their close structures and compositions. As mentioned above, the $R_3Ni_5Al_{19}$ IMC was observed during crystallization of {Y, Gd}–Ni–Al amorphous alloys [2]. But these results disagree with the results reported in [10]. The large amount of work performed by Raggio *et al.* (62 alloys, annealed at 773 K and 1073 K for 2-4 weeks, were analyzed by X-ray phase analysis, electron microscopy and microprobe analysis) resulted in the phase diagram

Table 1 Aluminium-rich binary phases with Ni, Gd and Y: crystal structure data.

IMC	Space group	Structure type	Lattice parameters, nm			Ref.
			a	*b*	*c*	
$NiAl_3$	*Pnma*	Fe_3C	0.65982	0.73515	0.48021	[3]
Ni_2Al_3	*P*-3*m*1	Ni_2Al_3	0.40282	–	0.48906	[3]
$GdAl_3$	$P6_3/mmc$	Mg_3Cd	0.6320	–	0.4592	[4]
$GdAl_2$	*Fd*-3*m*	$MgCu_2$	0.79020	–	–	[5]
YAl_3	*R*-3*m*	$BaPb_3$	0.6204	–	2.1184	[6]
YAl_2	*Fd*-3*m*	$MgCu_2$	0.7827	–	–	[7]

Table 2 Aluminium-rich ternary compounds in the {Y, Gd}–Ni–Al ternary systems: crystal structure data.

IMC	Space group	Structure type	Lattice parameters, nm			Ref.
			a	*b*	*c*	
$Gd_4Ni_6Al_{23}$	*C*2/*m*	$Y_4Ni_6Al_{23}$	1.5856	0.4078 β = 113.01°	1.8286	[12]
$Gd_3Ni_5Al_{19}$	*Cmcm*	$Gd_3Ni_5Al_{19}$	0.40893	1.5993	2.7092	[11]
$GdNi_3Al_9$	*R*32	YNi_3Al_9	0.73006	–	2.7478	[14]
$GdNiAl_4$	*Cmcm*	$YNiAl_4$	0.4087	1.530	0.669	[15]
$Y_4Ni_6Al_{23}$	*C*2/*m*	$Y_4Ni_6Al_{23}$	1.5836	0.40681 β = 112.97°	1.8311	[13]
$Y_3Ni_5Al_{19}$	*Cmcm*	$Gd_3Ni_5Al_{19}$	0.408	1.598	2.689	[16]
YNi_3Al_9	*R*32	YNi_3Al_9	0.72894	–	2.7430	[14]
$YNiAl_4$	*Cmcm*	$YNiAl_4$	0.408	1.544	0.662	[17]

shown in Fig. 1. The authors reported the existence of the $Y_4Ni_6Al_{23}$ IMC in the Y–Ni–Al system at 773 K. But there are some inconsistencies between the nominal composition of the alloys and the corresponding phase equilibria (see Fig. 1 and the following comments). The alloy No. 44 of nominal composition $Y_{14.7}Ni_{14.7}Al_{70.6}$ was reported to be single phase <$Y_4Ni_6Al_{23}$>, although according to the reported phase diagram it should contain two phases <$Y_4Ni_6Al_{23}$ + YAl_3>. Similar disagreement occurred in the data for some other alloys: No. 37, No. 45, No. 46a, No. 49, No. 52a, No. 53a, No. 56(a,c) (see [10]).

A possible reason of these discrepancies could be a shift of the nominal composition of the samples in the range from ~0.5 to 4 at.% for different alloys. Another probable reason could be insufficient thermal treatment of the investigated alloys: 2 weeks at 773 K in [10-13] and 0.5-48 hours at 773 K in [16,18], which led us to the conclusion that these alloys were not homogenous.

The aim of this work was to reinvestigate the phase equilibria in the {Y, Gd}–Ni–Al systems at 773 K in the range 65-100 at.% Al and to find out if the crystallization of $Y_5Ni_8Al_{87}$ AMA (*R* = Y, Gd) leads to the precipitation of thermodynamically stable phases. The latter issue will provide deeper insight into the understanding of the mechanisms of crystallization of Al-based *R*–Ni–Al amorphous alloys and the effects of doping by other *R* and *M* elements to obtain AMA with defined properties.

Experimental details

Metals of the following purity were used (in wt.%): Gd 99.99, Y 99.95, Ni 99.99, Al 99.99. The samples were prepared in an arc-melting furnace from the initial metals under an argon atmosphere

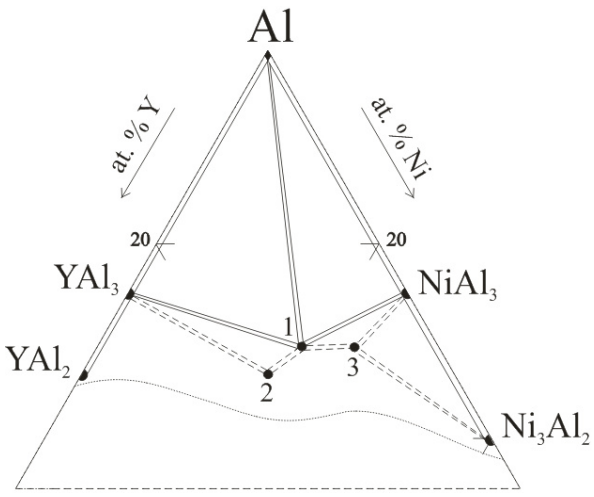

Fig. 1 Isothermal cross-section of the Y–Ni–Al ternary system at 773 K, nominal composition of some alloys and their numbers are according to [10]. Ternary compounds: 1 – $Y_4Ni_6Al_{23}$, 2 – $YNiAl_4$, 3 – YNi_3Al_9.

Table 3 Nominal (at.%) and phase composition of the investigated alloys in the Y–Ni–Al ternary system at 773 K.

No. of alloy	Nominal composition			Phases
	Y	Ni	Al	
1a	5	8	87	Al + $Y_3Ni_5Al_{19}$
2a	10	10	80	Al + YAl_3 + $Y_4Ni_6Al_{23}$
3a[1]	5	15	80	Al + $NiAl_3$ + YNi_3Al_9
4a	3	20	77	Al + $NiAl_3$ + YNi_3Al_9
5a	16	8	76	Al + YAl_3 + $Y_4Ni_6Al_{23}$
6a	8	18	74	Al + $Y_3Ni_5Al_{19}$ + YNi_3Al_9
7a[1]	13	14	73	Al + YAl_3 + $Y_4Ni_6Al_{23}$
8a	6	21	73	Al + $NiAl_3$ + YNi_3Al_9
9a[1]	17	11	72	YAl_3 + $Y_4Ni_6Al_{23}$
10a	11	17	72	$Y_3Ni_5Al_{19}$
11a	24	6	70	YAl_2 + YAl_3 + $YNiAl_4$
12a	11.75	18.25	70	$Y_4Ni_6Al_{23}$ + $Y_3Ni_5Al_{19}$ + YNi_3Al_9
13a	10	20	70	$Y_4Ni_6Al_{23}$ + $Y_3Ni_5Al_{19}$ + YNi_3Al_9
14a	12.1	18.2	69.7	$Y_4Ni_6Al_{23}$ + YNi_3Al_9 + $YNiAl_4$
15a[2]	10	20.5	69.5	$Y_4Ni_6Al_{23}$ + YNi_3Al_9 + $YNiAl_4$
16a	7.5	23	69.5	Ni_2Al_3 + YNi_3Al_9
17a	16	15	69	YAl_3 + $Y_4Ni_6Al_{23}$ + $YNiAl_4$
18a	3	28	69	$NiAl_3$ + Ni_2Al_3 + YNi_3Al_9
19a	12.5	19	68.5	$Y_4Ni_6Al_{23}$ + YNi_3Al_9 + $YNiAl_4$
20a	16.7	16.7	66.7	$YNiAl_4$
21a[3]	11	23	66	Ni_2Al_3 + YNi_3Al_9 + $YNiAl_4$
22a[3]	8	26	66	Ni_2Al_3 + YNi_3Al_9 + $YNiAl_4$
23a	13.5	21.5	65	Ni_2Al_3 + $YNiAl_4$

3a[1], 7a[1], 9a[1] contain traces of $Y_3Ni_5Al_{19}$; 15a[2] traces of Ni_2Al_3; 21a[3], 22a[3] traces of $Y_4Ni_6Al_{23}$.

(99.998 vol.%) on a water-cooled copper hearth with a W electrode. The samples were weighed on a torsion balance with the accuracy 0.002 g. Homogenization of the samples was performed in evacuated silica tubes at 773 K for 2-4 months. After the heat treatment the ampoules with the samples were quenched in cold water. X-ray diffraction (XRD) phase analysis was based on data obtained on DRON-2.0 (Fe K_α radiation, 2θ 15-115°, step 0.025°) and STOE STADI P (Cu K_α radiation, 2θ 6-120°, step 0.015°) powder diffractometers, using PCW [19] and FullProf [20] programs. Electron scanning microscopy and X-ray microprobe analyses (microscope REMMA-102-02, accuracy 1-5 at.%) were also performed.

Results and discussion

In total 23 and 20 alloys were prepared and investigated in the Y- and Gd-containing *R*–Ni–Al ternary systems. Their nominal and phase compositions are presented in Tables 3 and 4.

XRD patterns of the as-cast and annealed $Y_5Ni_8Al_{87}$ samples are presented in Fig. 2. The Rietveld profile analysis revealed two phases in the as-cast alloy: Al and $Y_4Ni_6Al_{23}$ ternary IMC (Fig. 2a). After the heat treatment of the alloy at 773 K for 4 months, the profile analysis showed the presence of Al and another ternary compound: $Y_3Ni_5Al_{19}$ (structure type $Gd_3Ni_5Al_{19}$) (see Fig. 2b). Both samples (as-cast and annealed) were refined as a mixture of Al and $Y_4Ni_6Al_{23}$, and also as Al and $Y_3Ni_5Al_{19}$. The best refinements are presented in Fig. 2 (the as-cast alloy refined as Al and $Y_3Ni_5Al_{19}$ had residuals R_p, R_{wp} > 50 %; the annealed alloy refined as Al and $Y_4Ni_6Al_{23}$ had R_p, R_{wp} > 50 % too).

A similar structure transformation was observed in the sample No. 1b $Gd_5Ni_8Al_{87}$ after the same heat treatment: Al and $Gd_4Ni_6Al_{23}$ IMC were found in the as-cast sample (Fig. 3a), whereas after annealing Al and the $Gd_3Ni_5Al_{19}$ ternary compound with traces of $Gd_4Ni_6Al_{23}$ were observed (Fig. 3b). These XRD profiles were also refined with the assumption of co-existence of two ternary IMC structures: $Gd_3Ni_5Al_{19}$ and $Gd_4Ni_6Al_{23}$. The best refinements are presented in Fig. 3 (the as-cast alloy refined as Al and $Gd_3Ni_5Al_{19}$ had residuals R_p, R_{wp} > 50 %; the annealed alloy refined as Al and $Y_4Ni_6Al_{23}$ had R_p = 2.12%, R_{wp} = 3.78%, and the same alloy refined as Al and $Gd_3Ni_5Al_{19}$ had R_p = 3.03 %, R_{wp} = 3.87%; the refinement considering a three-phase sample with the minimal R_p, R_{wp} was chosen).

Such changes in the phase content during the heat treatment indicate that the $R_4Ni_6Al_{23}$ IMC with the $Y_4Ni_6Al_{23}$ structure type exists in inhomogeneous samples in certain ranges of the phase diagram. This could be the reason for the above-mentioned discrepancies in the literature: the IMC compound with $Gd_3Ni_5Al_{19}$-type structure is not observed in relatively briefly heat-treated alloys.

Table 4 Nominal (at.%) and phase composition of the investigated alloys in the Gd–Ni–Al ternary system at 773 K.

No. of alloy	Nominal composition			Phases
	Gd	Ni	Al	
1b	5	8	87	Al + $Gd_3Ni_5Al_{19}$
2b[1]	10	10	80	Al + $GdAl_3$ + $Gd_4Ni_6Al_{23}$
3b	5	15	80	Al + $NiAl_3$ + $Gd_3Ni_5Al_{19}$
4b	3	20	77	Al + $NiAl_3$ + $Gd_3Ni_5Al_{19}$
5b	16	8	76	Al + $GdAl_3$ + $Gd_4Ni_6Al_{23}$
6b	8	18	74	Al + $NiAl_3$ + $Gd_3Ni_5Al_{19}$
7b	6	21	73	$NiAl_3$ + $Gd_3Ni_5Al_{19}$
8b	17	11	72	$GdAl_3$ + $Gd_4Ni_6Al_{23}$ + $GdNiAl_4$
9b	11	17	72	$Gd_3Ni_5Al_{19}$
10b	24	6	70	$GdAl_3$ + $GdAl_2$ + $GdNiAl_4$
11b	11.75	18.25	70	$Gd_4Ni_6Al_{23}$ + $Gd_3Ni_5Al_{19}$ + $GdNi_3Al_9$
12b	10	20	70	$Gd_4Ni_6Al_{23}$ + $Gd_3Ni_5Al_{19}$ + $GdNi_3Al_9$
13b	12.1	18.2	69.7	Ni_2Al_3 + $Gd_4Ni_6Al_{23}$ + $GdNiAl_4$
14b	7.5	23	69.5	Ni_2Al_3 + $Gd_4Ni_6Al_{23}$ + $GdNi_3Al_9$
15b	16	15	69	$GdAl_3$ + $Gd_4Ni_6Al_{23}$ + $GdNiAl_4$
16b[1]	3	28	69	$NiAl_3$ + Ni_2Al_3 + $GdNi_3Al_9$
17b	16.7	16.7	66.7	$GdNiAl_4$
18b	11	23	66	Ni_2Al_3 + $Gd_4Ni_6Al_{23}$ + $GdNiAl_4$
19b[2]	8	26	66	Ni_2Al_3 + $Gd_4Ni_6Al_{23}$ + $GdNi_3Al_9$
20b	11.5	24	64.5	Ni_2Al_3 + $GdNiAl_4$

2b[1], 16b[1] contain traces of $Gd_3Ni_5Al_{19}$; 19b[2] traces of $GdNiAl_4$.

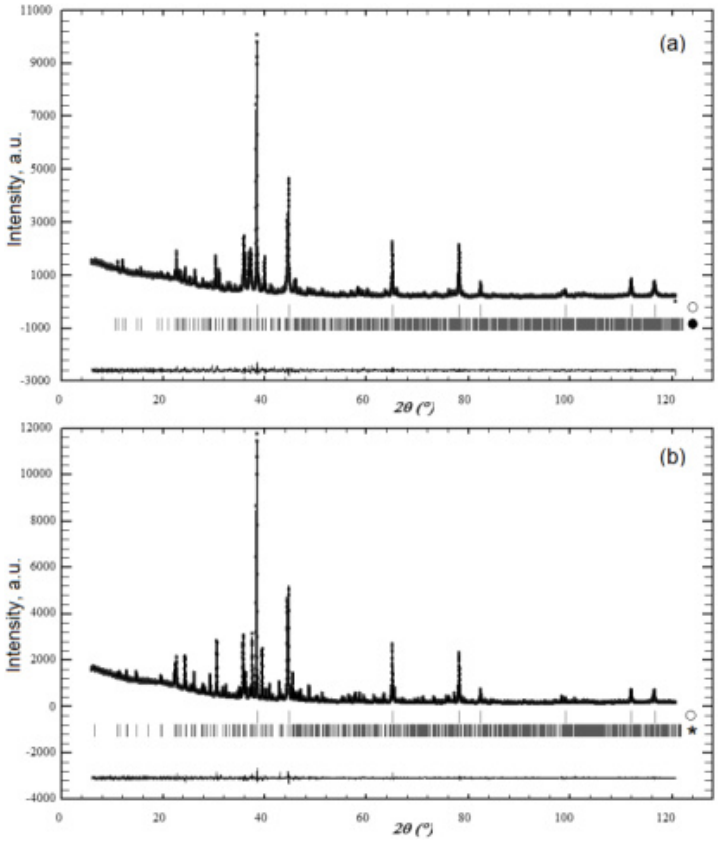

Fig. 2 XRD patterns of the as-cast (a) and heat-treated (b) sample No. 1a $Y_5Ni_8Al_{87}$ and the difference diagram (bottom) (STOE STADI P diffractometer, Cu K_α radiation). Positions of the Bragg reflections: (a) Al (○) and $Y_4Ni_6Al_{23}$ (●) (R_p = 3.98 %, R_{wp} = 5.44 %); (b) Al (○) and $Y_3Ni_5Al_{19}$ (*) (R_p = 3.75 %, R_{wp} = 5.12 %).

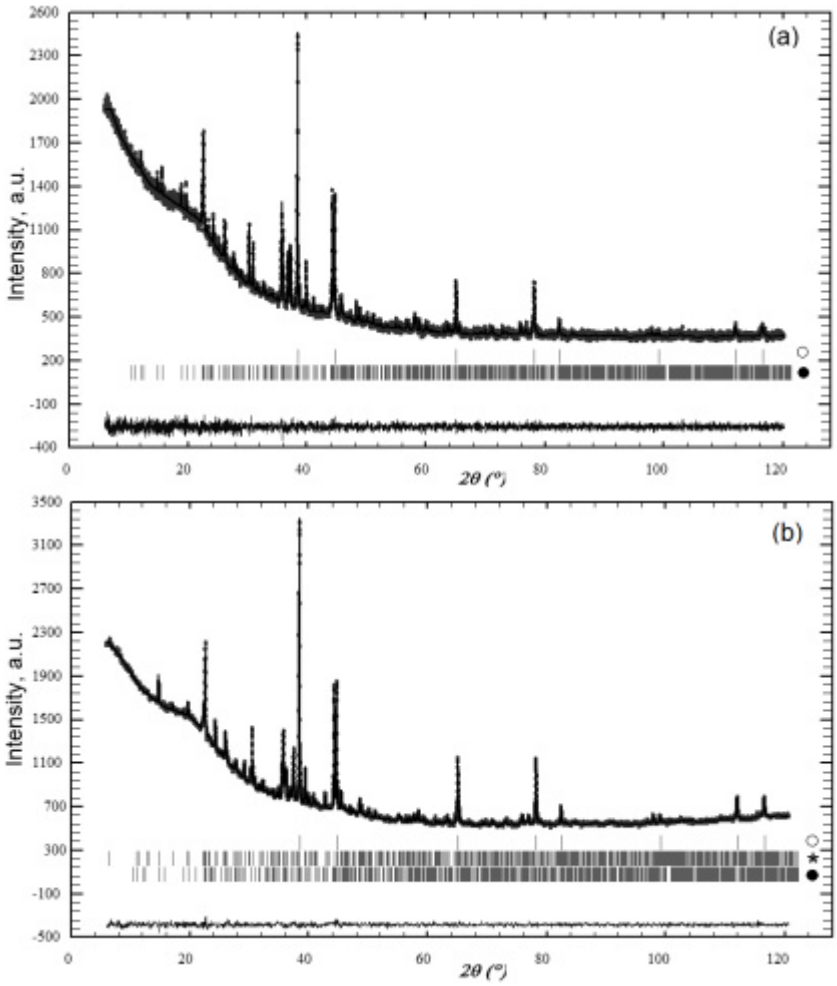

Fig. 3 XRD patterns of the as-cast (a) and heat-treated (b) sample No. 1b $Gd_5Ni_8Al_{87}$ and the difference diagram (bottom) (STOE STADI P diffractometer, Cu K_α radiation). Positions of the Bragg reflections: (a) Al (○) and $Gd_4Ni_6Al_{23}$ (●) (R_p = 2.15 %, R_{wp} = 2.80 %); (b) Al (○), $Gd_3Ni_5Al_{19}$ (*) and $Gd_4Ni_6Al_{23}$ (●) (R_p = 1.14 %, R_{wp} = 1.48 %).

Taking into account that the structure types $Gd_3Ni_5Al_{19}$ and $Y_4Ni_6Al_{23}$ have similar structure and are close to each other in composition, Vasiliev *et al.* [16,18] suggest that these compounds are polymorphic modifications of the same intermetallic compound. However, exact compositions are reported for these IMC in the literature [11-13]. Taking into account that the IMC with $Y_4Ni_6Al_{23}$-type structure is observed in as-cast alloys, one can suggest that the structure type $Y_4Ni_6Al_{23}$ is a high-temperature modification. Rietveld refinements of a series of long-term annealed samples showed that the ternary IMC with this structure type is thermodynamically stable and is in equilibrium with other IMC. Figs. 4 and 5 show XRD patterns of such samples. Data on the phase composition of these two and other samples of the {Y, Gd}–Ni–Al ternary systems, based on the results of XRD phase analyses, are presented in Tables 3 and 4.

The experimental results indicate that the ternary IMC $R_4Ni_6Al_{23}$ and $R_3Ni_5Al_{19}$ (R = Y, Gd) are in equilibria with other binary and ternary IMC at 773 K and are thermodynamically stable.

Tables 5 and 6 show the results of the crystal structure refinement of $Y_3Ni_5Al_{19}$ from powder X-ray diffraction data. The crystal structure had previously been refined from single crystal XRD data and confirmed by electron microscopy [16]. The data from single crystal and powder XRD refinements are in good agreement.

The results of the X-ray phase analysis were also confirmed by electron microscopy and microprobe analysis. These results are presented in Figs. 6, 7 and in Table 7. The results of the microstructure, microprobe and XRD phase analyses are in good agreement. It should be pointed out that the microprobe method revealed traces of $Gd_3Ni_5Al_{19}$ in sample No. 16b $Gd_3Ni_{28}Al_{69}$ and some other samples (see Tables 3 and 4). Taking into account that the compounds with the $Gd_3Ni_5Al_{19}$-type structure are thermodynamically stable (could be obtained by long heat treatment of the as-cast alloys) and their

Table 5 Details of the structure refinement for the polycrystalline sample $Y_5Ni_8Al_{87}$ (STOE STADI P diffractometer, Cu K_α radiation).

Phase		$Y_3Ni_5Al_{19}$
Space group		*Cmcm*
Unit cell parameters	*a*, nm	0.40713(1)
	b, nm	1.5957(3)
	c, nm	2.7052(6)
	V, nm^3	1.7574(6)
Formula unit per cell *Z*		4
Density D_x, g cm^{-3}		4.790
Texture parameter *G*		1.335(3) [001]
FWHM parameters *U*, *V*, *W*		0.008(2), 0.012(2), 0.0047(5)
Mixing parameter η		0.58(3)
Asymmetry parameter C_M		-0.009(5)
Number of refined parameters		65
Reliability factors R_B, R_p, R_{wp}		0.0495, 0.0448, 0.0593
Goodness of fit *S*		1.13

Table 6 Atomic coordinates and isotropic displacement parameters for $Y_3Ni_5Al_{19}$ (powder data, structure type $Gd_3Ni_5Al_{19}$, Pearson symbol *oS*108, space group *Cmcm*, *a* = 0.40713(1), *b* = 1.5957(3), *c* = 2.7052(6) nm).

Atom	Wyckoff position	*x*	*y*	*z*	$B_{iso}\times10^2$, nm^2
Al1	8*f*	0	0.9639(5)	0.3250(4)	1.3(2)
Ni1	8*f*	0	0.9458(2)	0.4154(2)	1.2(1)
Al2	8*f*	0	0.9336(5)	0.9693(5)	1.6(2)
Y1	8*f*	0	0.8342(2)	0.8649(1)	1.14(6)
Al3	8*f*	0	0.7900(5)	0.4107(4)	1.0(2)
Al4	8*f*	0	0.7740(5)	0.3054(4)	1.4(2)
Al5	8*f*	0	0.7670(4)	0.9726(4)	0.5(2)
Ni2	8*f*	0	0.6582(2)	0.4582(2)	1.16(9)
Al6	8*f*	0	0.6305(4)	0.8659(4)	0.7(2)
Al7	8*f*	0	0.5937(4)	0.9625(4)	0.7(2)
Al8	8*f*	0	0.4637(5)	0.9002(4)	0.9(2)
Al9	8*f*	0	0.4216(5)	0.7993(4)	1.0(2)
Ni3	4*c*	0	0.0451(4)	¼	1.5(2)
Al10	4*c*	0	0.1934(7)	¼	1.3(3)
Y2	4*c*	0	0.3885(2)	¼	1.15(9)

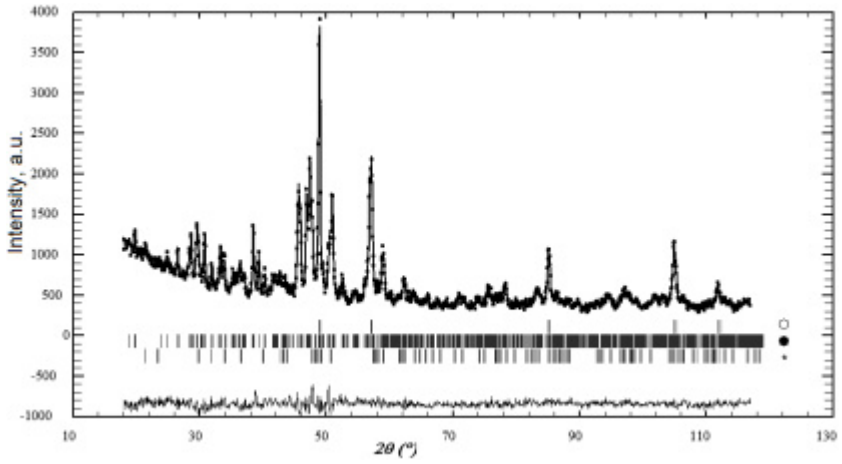

Fig. 4 XRD pattern of the annealed sample No. 2a $Y_{10}Ni_{10}Al_{80}$ and the difference diagram (bottom) (DRON-2.0 diffractometer, Fe K_α radiation). Positions of the Bragg reflections: Al (○), $Y_4Ni_6Al_{23}$ (●) and YAl_3 (*) (R_p = 4.65 %, R_{wp} = 5.99 %).

Table 7 Data of the X-ray microprobe analysis of the {Y, Gd}–Ni–Al ternary alloys.

No. of alloy	Nominal composition, at.%	Experimental composition, at.%			Phase
		R	Ni	Al	
4a	$Y_3Ni_{20}Al_{77}$	–	–	100	Al (dark)
		–	21	79	$NiAl_3$ (grey)
		20	5	74	YNi_3Al_9 (light)
13a	$Y_{10}Ni_{20}Al_{70}$	22	9	69	YNi_3Al_9 (grey)
		18	13	69	$Y_4Ni_6Al_{23}$ ($Y_3Ni_5Al_{19}$) (light)
19a	$Y_{12.5}Ni_{19}Al_{68.5}$	21	8	71	YNi_3Al_9 (dark)
		17	12	71	$Y_4Ni_6Al_{23}$ (grey)
		17	15	68	$YNiAl_4$ (light)
21a	$Y_{11}Ni_{23}Al_{66}$	21	10	69	YNi_3Al_9 (grey)
		16	14	70	$YNiAl_4$ (light)
3b	$Gd_5Ni_{15}Al_{80}$	–	–	100	Al (dark)
		–	28	72	$NiAl_3$ (grey)
		19	11	70	$Gd_3Ni_5Al_{19}$ (light)
4b	$Gd_3Ni_{20}Al_{77}$	–	–	100	Al (dark)
		–	22	78	$NiAl_3$ (grey)
		14	9	77	$Gd_3Ni_5Al_{19}$ (light)
16b	$Gd_3Ni_{28}Al_{69}$	–	30	70	$NiAl_3$ (dark)
		21	11	68	$Gd_3Ni_5Al_{19}$ ($Gd_4Ni_6Al_{23}$) (white)
		26	8	66	$GdNi_3Al_9$ (light grey)
		–	42	58	Ni_2Al_3 (grey)
19b	$Gd_8Ni_{26}Al_{66}$	22	9	69	$GdNi_3Al_9$ (grey)
		18	14	68	$Gd_4Ni_6Al_{23}$ (light)
		–	42	58	Ni_2Al_3 (dark)

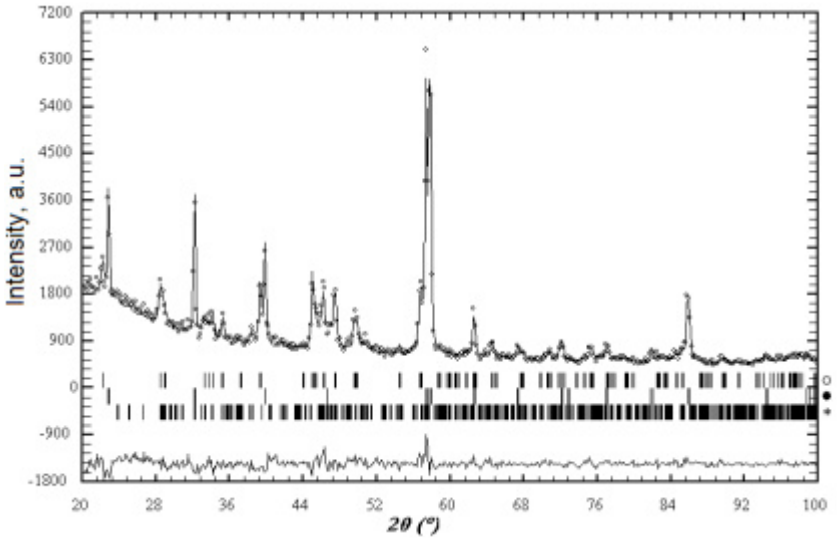

Fig. 5 XRD pattern of the annealed sample No. 14a $Gd_{12.1}Ni_{18.2}Al_{69.7}$ and the difference diagram (bottom) (DRON-2.0 diffractometer, Fe K_α radiation). Positions of the Bragg reflections: $NiGdAl_4$ (○), Ni_2Al_3 (●) and $Gd_4Ni_6Al_{23}$ (*) (R_p = 5.47 %, R_{wp} = 6.75 %).

traces are present in some ternary alloys, one can assume that this IMC is in peritectic equilibrium with other compounds, which makes it more difficult to reach the equilibrium state of the alloys, even by a long-term heat treatment.

Based on the obtained results the isothermal cross-section of the {Y, Gd}–Ni–Al ternary system at 773 K in the 65-100 at.% Al concentration range are shown in Figs. 8 and 9. These two phase diagrams are similar to each other, with only a few exceptions for the equilibria with the ternary compounds 1, 3 and 4. As it can be seen from Figs. 1, 8 and 9, some equilibria of the phase diagrams differ from those reported in [10]. An additional investigation of a few as-cast samples was carried out in order to confirm the equilibrium state of the investigated samples.

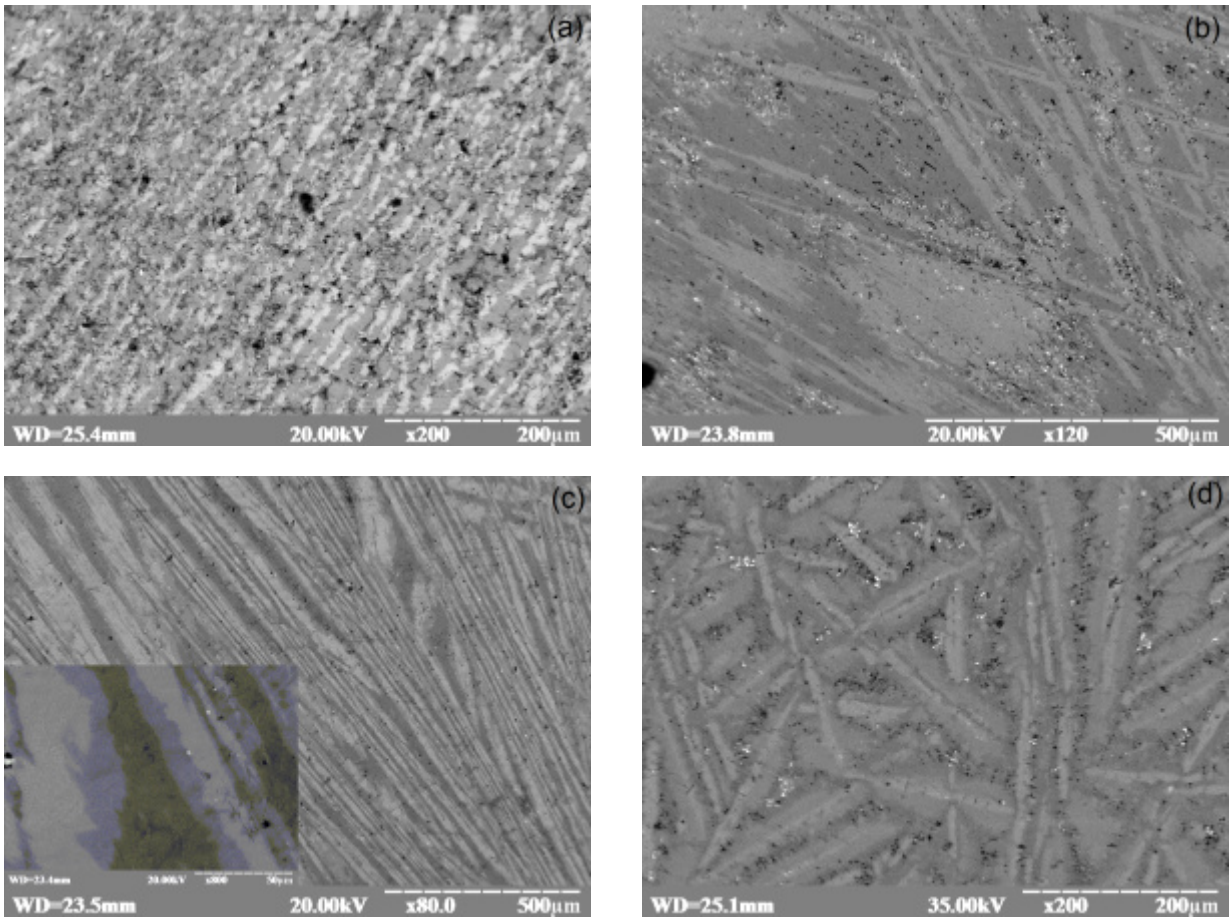

Fig. 6 Microstructures of Y–Ni–Al ternary alloys with the following composition:
(a) No. 4a $Y_3Ni_{20}Al_{77}$ <Al (dark) + $NiAl_3$ (grey) + YNi_3Al_9 (light)>; (b) No. 13a $Y_{10}Ni_{20}Al_{70}$ <YNi_3Al_9 (grey) + $Y_4Ni_6Al_{23}$ ($Y_3Ni_5Al_{19}$) (light)>; (c) No. 19a $Y_{12.5}Ni_{19}Al_{68.5}$ <$YNiAl_4$ (light) + YNi_3Al_9 (dark) + $Y_4Ni_6Al_{23}$ (grey)>; (d) No. 21a $Y_{11}Ni_{23}Al_{66}$ <Ni_2Al_3 (dark) + $YNiAl_4$ (light) + YNi_3Al_9 (grey)>.

Fig. 10a shows the XRD pattern of the as-cast sample No. 3a $Y_5Ni_{15}Al_{80}$, revealing the presence of three phases: Al, $NiAl_3$ and $Y_4Ni_6Al_{23}$, in agreement with the phase diagram reported in [10] (see Fig. 1). The XRD pattern of the same alloy annealed for 2 months shows changes in its phase content. After annealing Al, YNi_3Al_9, $NiAl_3$ and traces from $Y_3Ni_5Al_{19}$ are observed in the XRD pattern, presented in Fig. 10b.

A similar transformation occurred during the heat treatment of the sample No. 7b $Gd_6Ni_{21}Al_{73}$. Three phases, Ni_2Al_3, $NiAl_3$ and $Gd_4Ni_6Al_{23}$, are present in the as-cast alloy, but two phases, $NiAl_3$ and $Gd_3Ni_5Al_{19}$, were observed after two months annealing, as it can be seen from the XRD patterns (Fig. 11a,b). The results, presented in Figs. 10 and 11, indicate a strong influence of the heat treatment on the phase content of Al-rich {Y, Gd}–Ni–Al ternary alloys and explain some of the controversial literature data indicated in the Introduction.

Fig. 12 shows XRD patterns of an amorphous alloy $Y_5Ni_8Al_{87}$ prepared by the melt-spinning technique and afterwards totally crystallized by heating it up to 639 K at a heating rate of 20 K/min, and of an alloy of the same composition prepared by arc-melting and homogenized at 773 K for 4 months. The phase composition of these two alloys is the same. This result indicates that the amorphous alloy crystallizes according to the phase equilibrium diagram. Furthermore, the thermodynamically equilibrium crystalline state was reached after a very short time, 1 h, at 430 K. XRD data on $R_5Ni_8Al_{87}$ amorphous alloys (R = Y, Gd) and their crystallization procedure are presented in more detail in [2]. Similar results have been obtained for a $Gd_5Ni_8Al_{87}$ amorphous metallic alloy.

Conclusions

The phase equilibria in the Al-rich region of the {Y, Gd}–Ni–Al ternary systems at 773 K have been reinvestigated using XRD, microstructure and X-ray microprobe analysis. Four intermetallic compounds: 1 – $R_3Ni_5Al_{19}$ (structure type $Gd_3Ni_5Al_{19}$), 2 – $R_4Ni_6Al_{23}$ ($Y_4Ni_6Al_{23}$), 3 – RNi_3Al_9 (YNi_3Al_9),

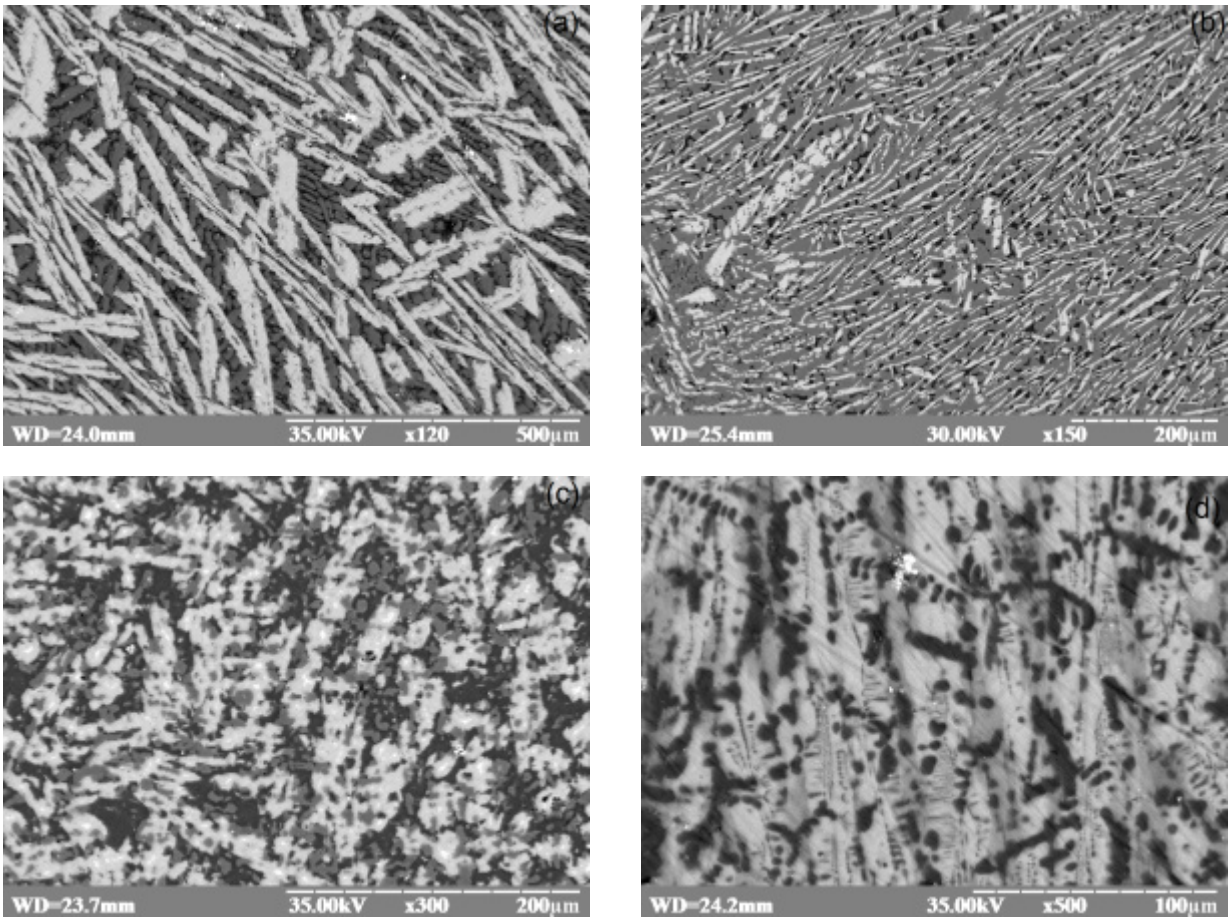

Fig. 7 Microstructures of Gd–Ni–Al ternary alloys with the following composition:
(a) No. 3b $Gd_5Ni_{15}Al_{80}$ <Al (dark) + $NiAl_3$ (grey) + $Gd_3Ni_5Al_{19}$ (light)>; (b) No. 4b $Gd_3Ni_{20}Al_{77}$ <Al (dark) + $NiAl_3$ (grey) + $Gd_3Ni_5Al_{19}$ (light)>; (c) No. 16b $Gd_3Ni_{28}Al_{69}$ <$NiAl_3$ (dark) + Ni_2Al_3 (grey) + $GdNi_3Al_9$ (light grey) + $Gd_3Ni_5Al_{19}$ (light)>; (d) No. 19b $Gd_8Ni_{26}Al_{66}$ <Ni_2Al_3 (dark) + $GdNi_3Al_9$ (grey) + $Gd_4Ni_6Al_{23}$ (light)>.

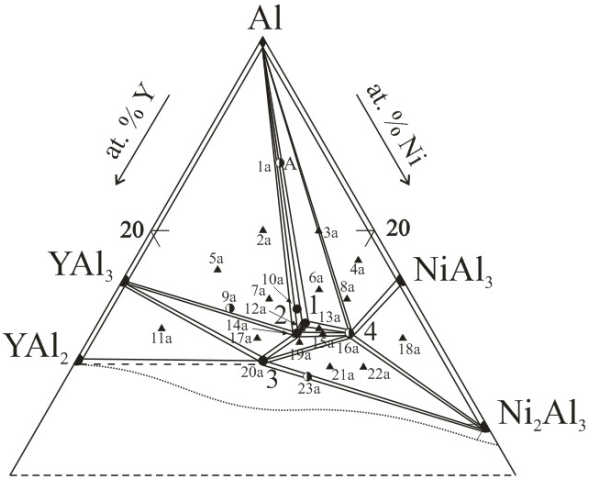

Fig. 8 Isothermal cross-section of the Y–Ni–Al ternary system at 773 K.
● single-phase sample, ◑ two-phase, ▲ three-phase; A – composition of alloy, which corresponds to the amorphous alloy $Y_5Ni_8Al_{87}$. Ternary compounds: 1 – $Y_3Ni_5Al_{19}$, 2 – $Y_4Ni_6Al_{23}$, 3 – $YNiAl_4$, 4 – YNi_3Al_9.

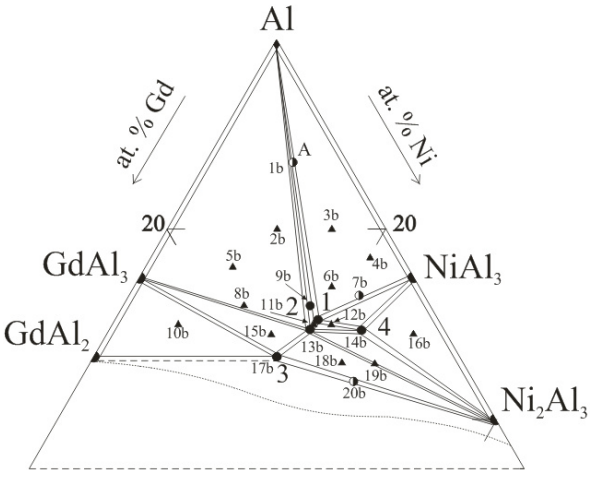

Fig. 9 Isothermal cross-section of the Gd–Ni–Al ternary system at 773 K.
● single phase sample, ◑ two-phase, ▲ three-phase; A – composition of alloy, which corresponds to the amorphous alloy $Gd_5Ni_8Al_{87}$. Ternary compounds: 1 – $Gd_3Ni_5Al_{19}$, 2 – $Gd_4Ni_6Al_{23}$, 3 – $GdNiAl_4$, 4 – $GdNi_3Al_9$.

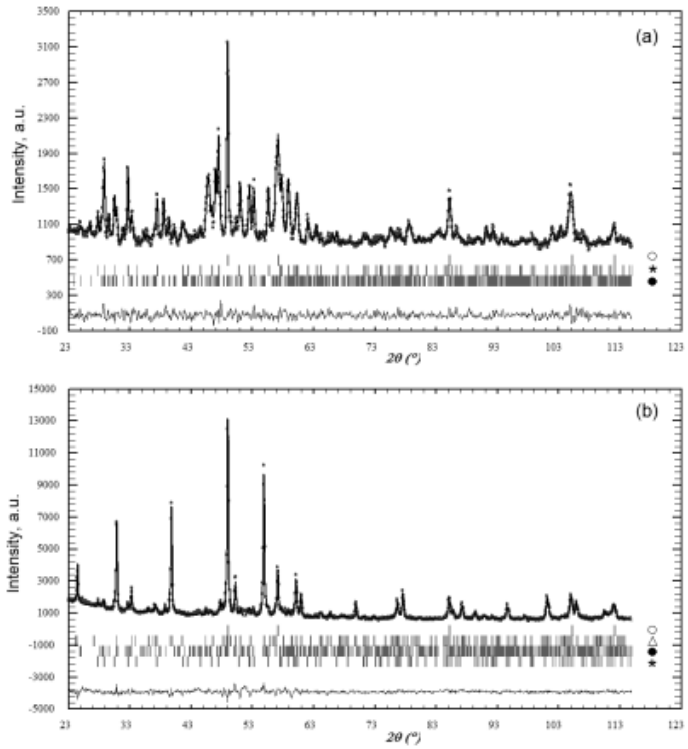

Fig. 10 XRD patterns of the as-cast (a) and annealed (b) sample No. 3a $Y_5Ni_{15}Al_{80}$ and the difference diagram (bottom) (DRON-2.0 diffractometer, Fe K_α radiation).
Positions of the Bragg reflections: (a) Al (○), $NiAl_3$ (*) and $Y_4Ni_6Al_{23}$ (●) (R_p = 2.49 %, R_{wp} = 3.18 %); (b) Al (○), YNi_3Al_9 (Δ), $Y_3Ni_5Al_{19}$ (●) and $NiAl_3$ (*) (R_p = 5.80 %, R_{wp} = 7.80 %).

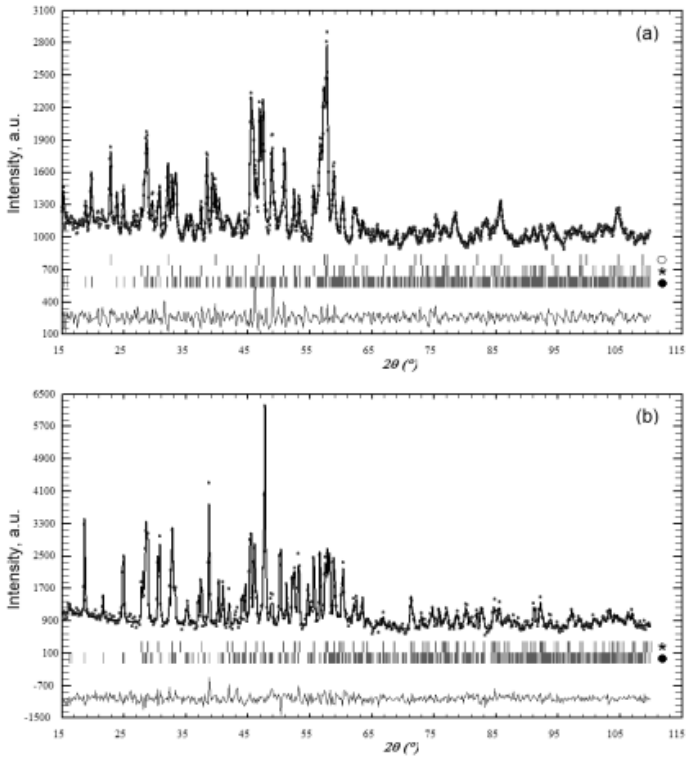

Fig. 11 XRD patterns of the as-cast (a) and heat-treated (b) sample No. 7b $Gd_6Ni_{21}Al_{73}$ and the difference diagram (bottom) (DRON-2.0 diffractometer, Fe K_α radiation).
Positions of the Bragg reflections: (a) Ni_2Al_3 (○), $NiAl_3$ (*) and $Gd_4Ni_6Al_{23}$ (●) (R_p = 2.77 %, R_{wp} = 3.62 %); (b) $NiAl_3$ (*) and $Gd_3Ni_5Al_{19}$ (●) (R_p = 5.92 %, R_{wp} = 7.57 %).

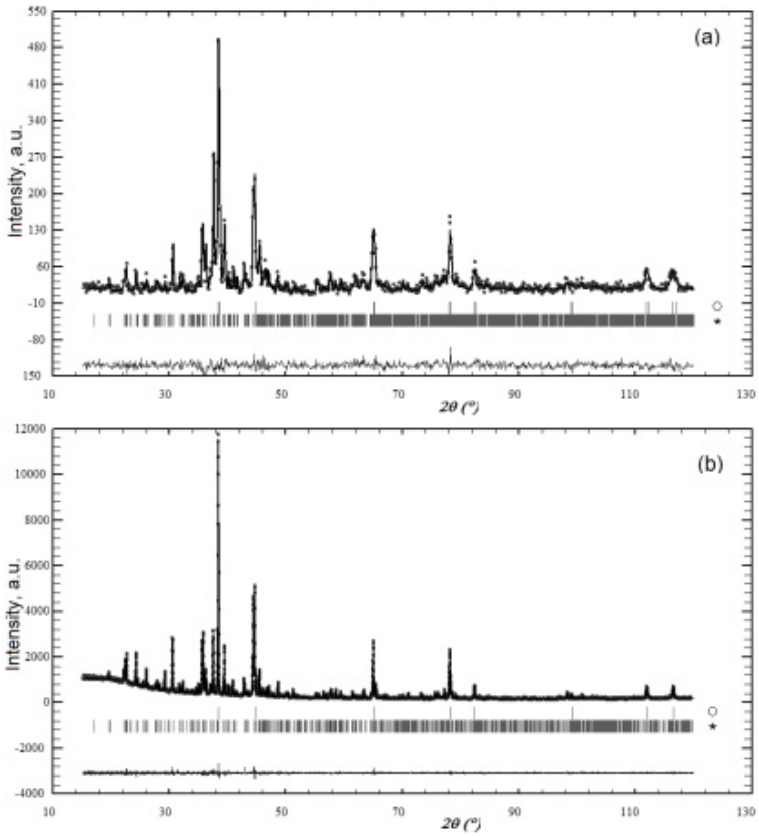

Fig. 12 XRD patterns of the amorphous alloy $Y_5Ni_8Al_{87}$ totally crystallized after heating [2] (a) and its crystalline arc-melted analogue (b) and the difference diagrams (bottom).
Positions of the Bragg reflections: Al (○) and $Y_3Ni_5Al_{19}$ (*); (a) R_p = 14.8 %, R_{wp} = 19.7 % (Philips X-Pert diffractometer, Cu K_α radiation); (b) R_p = 3.75 %, R_{wp} = 5.12 % (STOE STADI P diffractometer, Cu K_α radiation).

and 4 – RNiAl$_4$ (YNiAl$_4$), exist in both systems. It was shown that the thermodynamic equilibrium state of the samples could be reached by a long-term heat treatment (up to four months). Insufficient annealing time is probably the main reason for some controversial literature data on the {Y, Gd}–Ni–Al phase diagrams. The crystal structure of the $Y_3Ni_5Al_{19}$ ternary compound (space group *Cmcm*) was refined by the Rietveld method from X-ray powder diffraction data. The refined cell parameters are a = 0.40713(1) nm, b = 1.5957(3) nm, c = 2.7052(6) nm.

The crystallization of $R_5Ni_8Al_{87}$ (R = Y, Gd) amorphous metallic alloys leads to thermodynamical equilibrium after a very short time (a few hours at 703 K), in contrast to crystalline arc-melted samples, which need a much longer heat treatment (up to 4 months at 773 K).

References

[1] A. Inoue, *Prog. Mater. Sci.* 43 (1998) 365-520.
[2] T. Mika, M. Karolus, G. Haneczok, L. Bednarska, E. Łagiewka, B. Kotur, *J. Non-Cryst. Solids* 354 (2008) 3099-3106.
[3] A.J. Bradley, A. Taylor, *Philos. Mag.* 23 (1937) 1049-1067.
[4] J.H.N. Van Vucht, K.H.J. Buschow, *J. Less-Common Met.* 10 (1966) 98-107.
[5] N.C. Baenziger, J.L. Moriarty Jr., *Acta Crystallogr.* 14 (1961) 948-950.
[6] D.M. Bailey, *Acta Crystallogr.* 23 (1967) 729-733.
[7] P.I. Kripyakevich, *Kristallografiya* 5 (1960) 440-441.
[8] R.M. Rykhal, O.S. Zarechnyuk, *Dopov. Akad. Nauk Ukr. RSR* 4 (1977) 375-377.
[9] R.M. Rykhal, O.S. Zarechnyuk, O.M. Marych, *Dopov. Akad. Nauk Ukr. RSR* 9 (1978) 853-854.
[10] R. Raggio, G. Borzone, R. Ferro, *Intermetallics* 8 (2000) 247-257.
[11] R.E. Gladyshevskii, K. Cenzual, E. Parthé, *J. Solid State Chem.* 100 (1992) 9-15.
[12] R.E. Gladyshevskii, E. Parthé, *Z. Kristallogr.* 198 (1992) 171-172.
[13] R.E. Gladyshevskii, E. Parthé, *Acta Crystallogr. C* 48 (1992) 232-236.
[14] R.E. Gladyshevskii, K. Cenzual, H.D. Flack, E. Parthé, *Acta Crystallogr. B* 49 (1993) 468-474.
[15] R.M. Rykhal, O.S. Zarechnyuk, G.V. Pyshchyk, *Dopov. Akad. Nauk Ukr. RSR* 9 (1973) 568-569.

[16] A.L. Vasiliev, M. Aindow, M.J. Blackburn, T.J. Watson, *Intermetallics* 12 (2004) 349-362.
[17] R.M. Rykhal, O.S. Zarechnyuk, Ya.P. Yarmolyuk, *Kristallografiya* 17(3) (1972) 521-523.
[18] A.L. Vasiliev, M. Aindow, T.J. Watson, M.J. Blackburn, *Intermetallics* 13 (2005) 741-748.
[19] W. Kraus, G. Nolge, *PowderCell for Windows*, Federal Institute for Materials Research and Testing, Berlin, 2000.
[20] J. Rodriguez-Carvajal, *Program FullProf*, Laboratoire Léon Brillouin, CEA-CNRS, 1998.